Journal of The Electrochemical Society, 2021 **168** 020519

Impact of Silicon Content within Silicon-Graphite Anodes on Performance and Li Concentration Profiles of Li-Ion Cells using Neutron Depth Profiling

Erfan Moyassari,[1,z] Luiza Streck,[1] Neelima Paul,[2] Markus Trunk,[2,3] Robert Neagu,[3] Chia-Chin Chang,[4] Shang-Chieh Hou,[5] Bastian Märkisch,[3] Ralph Gilles,[2] and Andreas Jossen[1,6]

[1]*Institute of Electrical Energy Storage Technology (EES), Technical University of Munich (TUM), 80333 Munich, Germany*
[2]*Heinz Maier-Leibnitz Zentrum (MLZ), Technical University of Munich (TUM), 85748 Garching, Germany*
[3]*Particle Physics at Low Energies, Physics Department, Technical University of Munich (TUM), 85748 Garching, Germany*
[4]*Department of Greenergy, National University of Tainan, Tainan, 70101, Taiwan*
[5]*Department of Materials Science and Engineering, National Cheng Kung University, Tainan, 70101, Taiwan*
[6]*Munich School of Engineering (MSE), Technical University of Munich (TUM), Lichtenbergstr. 4a, 85748 Garching, Germany*

Due to its high specific capacity, silicon is a promising candidate to substitute conventional graphite as anode material in lithium-ion batteries. However, pure silicon-based anodes suffer from poor capacity retention, mainly due to a large volume change during cycling, which results in material pulverization and other side reactions. Therefore, alternative compositions with lowered silicon content and a similar working voltage as graphite are favored, e.g. silicon-graphite (SiG), as they can reduce these volume change and side reactions while maintaining a high capacity. Here, neutron depth profiling (NDP) offers the unique possibility to quantify non-destructively the lithium concentration profile over the depth of these electrodes. In this study, the (de-)intercalation phenomena during (de-)lithiation in SiG porous anodes with silicon contents ranging from 0 wt% to 20 wt% is investigated for the first time using ex situ NDP during the initial discharge at defined depths of discharge (DODs) states. These findings are complemented by a conventional electrochemical analysis of the first full cycle with a charge/discharge rate of C/20. While the specific capacity is observed to increase with higher silicon content, NDP directly reveals a homogeneous irreversible lithium accumulation within the entire electrode depth.
 [DOI: 10.1149/1945-7111/abe1db]

Manuscript submitted December 9, 2020; revised manuscript received January 29, 2021. Published February 8, 2021.

One strategy to increase the energy density of lithium-ion batteries is to incorporate silicon into the anodic electrode. In contrast to physical intercalation of lithium into conventional graphite, silicon alloys with up to 4.4 lithium atoms per silicon atom, allowing the capacity of the composite electrode to exceed the theoretical capacity of LiC_6 (372 mAh g^{-1}) forming in graphite. In fact, the alloy displays a capacity about ten times larger (3590 mAh g^{-1}).[1] Silicon is also a favorable anode material compared to graphite due to its low cost, abundancy, non-toxicity and low discharge potential (≈ 370mV vs Li/Li^+).[2,3]

Despite these advantages, the usage of pure silicon as electrode active material is associated with considerable volume changes of up to 300%,[1] dependent on the state of charge. This causes mechanical stress on the material resulting in the decay of cycle stability, the cracking of particles and partial loss of contact with the current collector.[4,5] In addition, the formation of silicon compounds at the solid electrolyte interface (SEI) inhibits the (de-)lithiation process.[6] In graphite anodes, such side reactions (SEI growth) mainly occur during the initial cycles. However, in silicon-based anodes, there exists continuous formation of SEI by exposing new surface material to the electrolyte due to the large volume change. The formation of a stable SEI layer is crucial for a long battery cycle life; nevertheless, it becomes difficult for silicon-based electrodes to form a stable SEI because of the volume effects mentioned above. Consequently, the capacity of the material is lowered and the stabilization of the columbic efficiency is hindered.[7–9] Recently, we confirmed with a neutron scattering study on SiG composite electrodes that the cracking of silicon particles occurs not just on a local level but also over the entire electrode volume.[10] Moreover, the cracking of particles was observed in this study only for the ≈ 200 nm silicon particles but not for the graphite particles.[11] One strategy adopted in order to mitigate such phenomena is the control of particle size, where smaller nano-sized silicon particles could be utilized in order to avoid fracture and therefore improve the cycling performance.[8,12,13]

Our focus is on studying electrochemical performances (capacities) and determining lithium concentration profiles across the thickness of electrode coatings for anodes with various SiG compositions, and comparing them to conventional graphite anodes. Obtaining the lithium concentration profile helps to explore the transport and electrochemical reactions that occur during the (de-) lithiation processes.[14–16] Moreover, it helps to illustrate the reasons behind the capacity loss, the side-reactions initiated by silicon and the storage properties of lithium (Li). Understanding these effects should lead to the production of durable and efficient electrode materials, since Li-ion (de-)lithiation and diffusion through solids is the primary limiting factor in SiG anodes.[17,18]

Neutron depth profiling (NDP) is a technique where a planar surface is bombarded with thermal neutrons.[19] When a cold neutron beam (energy range 0.1–10 meV) hits the material, certain nuclides emit charge particles: ^{3}He, ^{6}Li, ^{10}B, ^{14}N, ^{17}O, ^{33}S, ^{35}Cl and ^{40}K. Due to its high detection sensitivity for ^{6}Li, NDP is well-suited to non-destructively quantify the lithium concentration profile across the electrode depth.[17,20] A lithium-containing sample, the following reaction takes place:

$$^6\mathrm{Li} + \mathrm{n} \rightarrow \alpha(2055.55\ \mathrm{keV}) + {}^3\mathrm{H}(2727.92\ \mathrm{keV}). \quad [1]$$

After neutron capture, alpha- (α) and triton (^{3}H) particles are produced at well-defined energies. Depending on the path length, the particles lose energy in the investigated material before they emanate the sample surface. The lithium concentration profile is then obtained from the spectrum of the residual particle energies. Due to the lower energy loss of the ^{3}H compared to that of the α particle, electrode thicknesses up to ≈ 50 μm could be investigated here using the ^{3}H spectrum.[14,21]

NDP is a broadly used technique on the research of lithium-ion batteries. Lv et al. used it on lithium metal anodes, to investigate the plating/stripping phenomena that takes place on the surface of such

[z]E-mail: erfan.moyassari@tum.de

electrodes. Due to its non-destructive properties, the morphology can be study in detail even during battery operation using *operando* NDP.[22] Liu and Co investigated parasitic losses happening in the first lithiation revealing chemical process that take place during (de-) lithiation processes.[23] In addition, Wetjen et al. investigated the lithium concentration across the thickness of the electrodes using a 35 wt% SiG electrode for both different states of charge (SOC) and depths of discharge (DOD) during the first (de-)lithiation cycle and found a depth-independent utilization of the active materials.[15]

Our work focuses on the impact of changing the silicon content in SiG electrodes on Li concentration profiles with respect to the DOD using an electrode composition with a higher active-non-active material ratio.

Experimental

As shown in Fig. 1, the negative electrodes were prepared with a variety of silicon/graphite ratios as active material components (see Table I). The active material content of the electrode samples containing silicon (self-developed mixture) and graphite (MG13AN, China Steel Chemical Co.) was kept 95 wt% based on the weight of the final electrode. There are different silicon/graphite wt% ratios of 05:90, 07:88, 10:85, 15:80, 20:75 and graphite as 00:95. Moreover, the slurry was prepared in a planetary mixer (G-Mixer 400S, Chia Mey Machinery Co.) consisting of 95 wt% silicon/graphite, 2 wt% Super P (MMM Carbon, Blegium), 2.50 wt% carboxymethyl cellulose (CMC, Sigma-Aldrich Co.) and 0.50 wt% of styrene butadiene rubber (SBR, Zeon Co.) in deionized water (35 wt% solid content), respectively. After the dry mixing of the silicon, graphite and Super P, the mixture was added in binder solution and then mixed at 500 rpm for 60 min to keep from agglomerating and guarantee a homogeneous dispersion of the slurry. In addition, SBR solution was added stepwise at a reduced rotation speed. Finally, the slurry was coated onto the 10 μm copper foil then dried in an oven at 90 °C for 1 h. The information regarding the particle size distribution as well as the Scanning Electron Microscope (SEM) images of the studied samples are presented in the Appendix in Figs. A·1 and A·2, respectively.

To conduct electrochemical analysis of the electrode samples, open circuit potential (OCP) measurements were performed using half cells. The SiG vs Li foil coin cells (Hohsen Corp., Japan) were composed of a single-side-coated SiG electrode (⌀14 mm) and two glass fiber (⌀16 mm) separators (VWR, USA) against a Li-metal foil with ⌀ ≈ 16 mm (Rockwood Lithium, USA). The electrolyte used for these half cells was a 1 M $LiPF_6$ in 1:1 (wt:wt) Ethylene Carbonate (EC)/Ethyl Methyl Carbonate (EMC) with 10 wt% Fluoroethylene Carbonate (FEC) (Solvionic, France) as an additive. The half cells were filled with 100 μl of electrolyte under ambient pressure inside the glovebox (M. Braun Inertgas-System GmbH).

The coin cells for the NDP measurements were prepared in the same way, but first they were fully lithiated at C/20 using constant-current

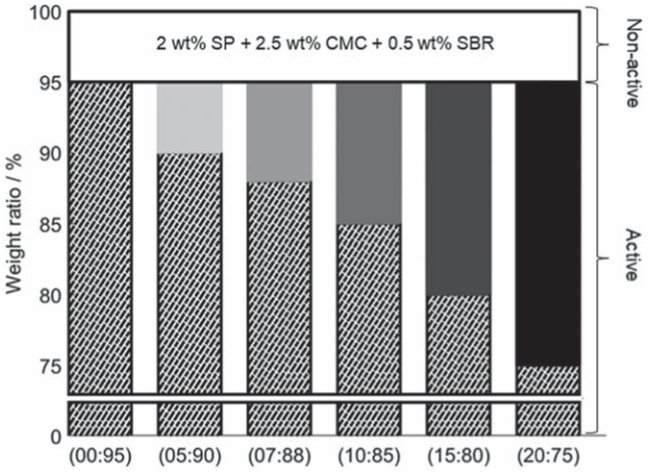

Figure 1. Composition of the different SiG electrodes. SP: carbon black as conductive agent, CMC: Carboxymethyl Cellulose as water-based binder and SBR represents Styrene-Butadiene Rubber as an additive. While the non-active material was kept at 5 wt% for all samples, the active composition was changed from 0 wt% up to 20 wt% silicon.

constant-voltage steps and then discharged to selected DODs (0%, 30%, 60% and 100%) using a constant-current rate (C-rate) of C/20. These measurements were done in a climate chamber (Vötsch Industrietechnik GmbH, Germany) at 25 °C using a battery cycler (CTS, Basytec GmbH, Germany). The data obtained for the electrochemical analysis contains an uncertainty of ±1.2%. The error was estimated based on the CTS technical data sheet[24] and the precision limitations of the equipment used for building the coin cells.

After cycling the coin cells to the desired DODs, the SiG electrodes were harvested from the cells inside a glovebox containing an argon atmosphere. Overall, six SiG compositions were used for the NDP experiment, each with four different DODs, resulting in 24 different samples. All electrodes were washed using dimethyl carbonate (DMC) in order to remove both the electrolyte residues and the separator. Afterwards the electrodes were dried, mounted on the NDP sample holder designed for this experiment and sealed in an aluminum foil pouch containing an argon atmosphere, avoiding any possible side reactions due to contact with air. The samples were then transported within 24 h to the NDP experiment, where the aluminum foil pouches were opened shortly before placing the samples in the vacuum atmosphere.[25] The NDP experiment is situated at the Prompt Gamma Activation Analysis (PGAA) facility of the Heinz Maier-Leibnitz Zentrum (MLZ) in Garching, Germany.[25,26] A cold neutron beam with a mean energy of 1.80 meV

Table I. Electrode composition properties. Data given in this table are calculated from the first full cycle at the C-rate of C/20 between 5 mV and 1.50 V.

Electrode properties	SiG (00:95)	SiG (05:90)	SiG (07:88)	SiG (10:85)	SiG (15:80)	SiG (20:75)
Theoretical electrode capacity [mAh]	1.33	2.61	2.71	3.82	4.15	4.96
Areal electrode capacity [mAh cm^{-2}]	0.86	1.70	1.76	2.49	2.70	3.22
Electrode mass loading [mg cm^{-2}]	2.57	3.28	2.98	3.55	3.06	3.03
Active material loading [mg_{AM} cm^{-2}]	2.44	3.12	2.83	3.38	2.91	2.88
Average electrode coating thickness [μm]	33.20	41.40	36.80	43.60	35.50	34.60
Electrode density [g cm^{-3}]	0.62	0.73	0.80	0.89	0.80	0.90
Electrode porosity [%]	71.68	67.22	64.39	60.04	64.39	60.09
Current for 1C [mA]	1.30	2.34	2.51	2.85	3.42	4.90
1st cycle coulombic efficiency [%]	91.45	93.35	91.34	83.62	93.13	95.08
1st cycle irreversible capacity [mAh_{irr} g_{AM}^{-1}]	36.02	35.70	60.95	120.85	58.61	48.49
1st cycle delithiation capacity [mAh g_{AM}^{-1}]	385.41	501.48	642.83	617.02	794.94	936.28
1st cycle lithiation capacity [mAh g_{AM}^{-1}]	421.43	537.18	703.78	737.87	853.55	984.77

and a thermal equivalent flux density 1.35×10^9 cm^{-2} s^{-1} irradiates the sample being in the center of the vacuum chamber at an angle of 45°.[14,26] A silicon surface-barrier detector is placed in parallel to the sample surface at a distance of ≈ 9.60 cm. A nominal 7.50-μm thick Kapton® foil was placed in front of the detector to separate the ^{3}H from the α particles.[21,27] The isolated ^{3}H energy spectrum was used as a measure of the lithium concentration profile within the electrodes. NDP data were obtained within 30–40 min per sample, depending on its lithium content. The signal rate was kept below 1000 s^{-1} using a beam attenuator of 47% for samples with high lithium content.[14,25,26] For a quantitative concentration analysis, the signal rate was compared to that of a reference standard (SRM2137 from NIST) being a silicon wafer with a known ^{10}B content.[28] Here, the cross sections of boron and lithium are taken into account and a natural ^{6}Li abundance (≈ 7.60%) is assumed. Error bars shown for NDP data in the figures include this correlated uncertainty from the calibration. For the concentration profiles, the energy loss of the triton particles in the probes is calculated using the SRIM (Stopping and Range of Ions in Matter) software, taking into account the different material compositions.[14,29]

Results and Discussion

The focus of this paper is on the first (dis-)charge cycle, specifically during the delithiation phase. The aim is to investigate the influence of silicon content in different electrode compositions on the (de-)lithiation process as well as on the (de-)intercalated lithium amount of the electrodes. As mentioned in the introduction, the commercialization of pure silicon anodes faces various obstacles, e.g. high-volume expansion and continuous decomposition of the electrolyte during (de-)lithiation. Repeated volume expansion causes mechanical fracturing and pulverization of the silicon particles inside the electrode mixture.[6,8,14] This further leads to the isolation of, or damage to, both the active materials and the electrical contacts, leading to a significant decrease in the reversible capacity of the silicon-based anodic electrode.[8,14] Such effects are expected to be less severe for the whole electrode with a lower silicon content in the electrode. Therefore, we investigate silicon-graphite composite electrodes, where the high theoretical capacity of silicon is combined with the established cycling stability of conventional graphite. Here, two approaches are used for the same set of electrode compositions: (I) Electrochemical analyses and (II) NDP analyses. First, the electrochemical analyses is discussed in the following.

(I) Electrochemical analyses.—In Fig. 2a the potential curves during the first full cycle for the different SiG electrodes are shown. The comparison of the (de-)lithiation of the different electrode compositions shows clear differences in their electrochemical behaviors. As expected, the value of specific capacity increases with the silicon content in the anodic active material composition. A specific experimental capacity of approx. 985 mAh g_{AM}^{-1} can be achieved for the SiG (20:75) after the first lithiation process, which is in good agreement with the values presented in earlier studies.[16] Table I lists the most important properties of the electrode compositions in order to give an overview of the investigated samples. Active material composition (in wt%) of the electrodes are described using the numbers in parentheses, e.g. SiG (00:95) demonstrates 0 wt% of silicon and 95 wt% of graphite. The measured lithiation capacities with increasing silicon content are in accordance to that expected based on the average electrode coating thickness and active material loadings. Moreover, the measured specific delithiation capacities increase with higher silicon content, as expected. Only for SiG (10:85) a higher irreversible capacity is measured, originating from the electrode preparation procedure and used cycling performance additives, e.g. pitch.

It is worth mentioning that increasing the silicon content of electrode compositions weakens the characteristic potential plateaus displayed by graphite. In order to observe the impact of the increasing silicon content, incremental current analysis (ICA) of the electrodes was conducted for the first full cycle, both for pure graphite and various SiG composite electrodes, and is presented in Fig. 2b. The peaks observed in the voltage windows between 0.25 and 0.10 V during the lithiation and from 0.05 to 0.15 V during the delithiation process are characteristic for the (de-)lithiation processes attributed to graphite. These peaks flatten out as the silicon content in the electrodes increases. In addition, there are some broad peaks between 0.20 and 0.32 V during the delithiation process. These features can be attributed to the growth of residual silicon clusters merging from smaller and medium-sized clusters to larger silicon domains and the peaks increase with higher silicon content.[30]

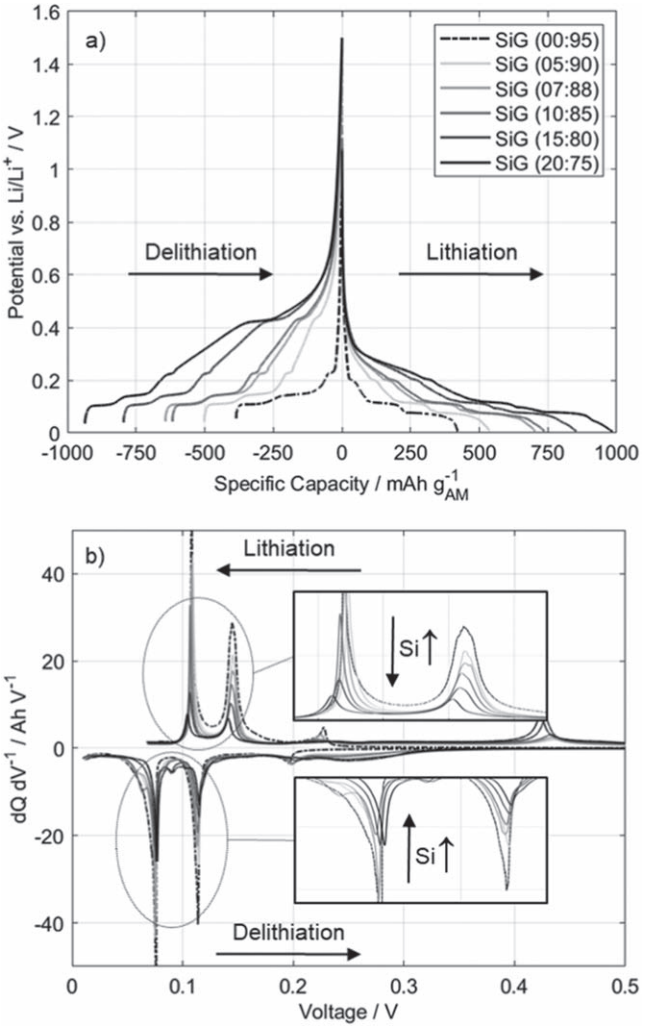

Figure 2. (a) Voltage vs specific capacity for 1st full-cycle (b) ICA curves for 1st full-cycle for different SiG composite electrodes with 5 mV as lithiation cutoff condition and at the same C-rate of C/20.

Wetjen et al. states that the delithiation of graphite occurs at potentials up to ≈ 0.20 V lower than needed for the delithiation of silicon.[15] At the same time, the ICA analysis from Fig. 2b demonstrates that, higher silicon ratios result in less dominant characteristic graphite peaks at voltages lower than 0.20 V and reveals coexistence of peaks at higher voltages. This implies that the electrochemical behaviors of silicon and graphite as electrode active materials cannot be considered independent from one another in the studied potential window.

The net capacity (Q_{net}) can be interpreted as lithium content -active and inactive- situated in the electrode, after delithiation to specific DODs. The total -active and inactive- lithium mass (m_{Li}) can be calculated using the following equations:

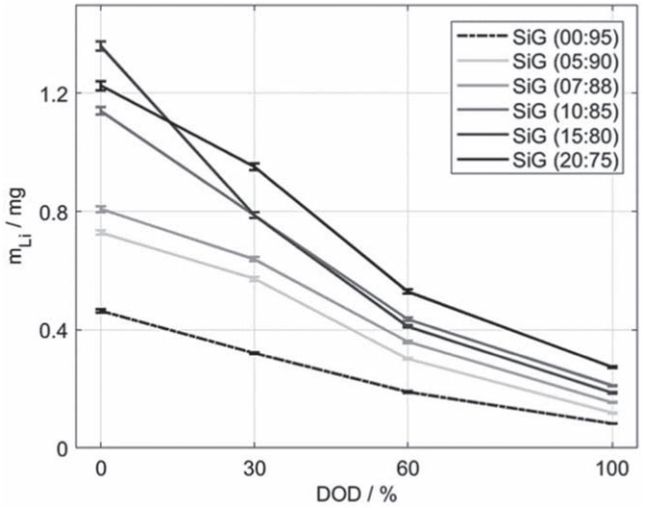

Figure 3. Total lithium mass (m_{Li}) within the electrodes at different DODs calculated using electrochemical analysis with an uncertainty of ±1.2%.

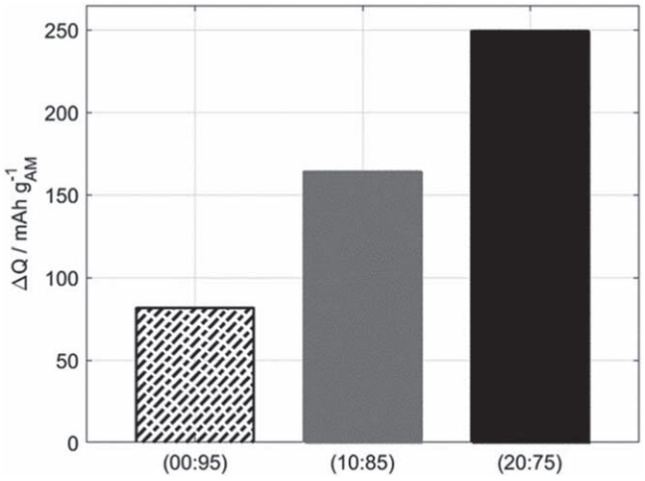

Figure 4. Capacity loss due to SEI formation for three different SiG compositions, calculated using the difference between the capacity at the end of initial SEI formation and the capacity at 100% DOD.

$$Q_{net} = Q_{Lithiation} - Q_{Delithiation} \quad [2]$$

and

$$m_{Li} = \frac{Q_{net} \times M_{Li}}{n \times F} = \frac{Q_{net} \times 6.94\ gmol^{-1}}{1 \times 96485\ Asmol^{-1}}, \quad [3]$$

where Q_{net} is the absolute amount of charge inside an electrode, calculated using the lithiation and delithiation charges.[15] M_{Li} is the atomic mass of lithium, n is the amount of electrons exchanged during reaction and F is Faraday's constant. We also consider that for every electron exchanged, one lithium atom is transferred to one electrode for intercalation or SEI growth. Figure 3 shows the accumulation of lithium mass incorporated into each electrode composition at different DODs. The necessary data are extracted from the pre-measurements elaborated in the experimental section. In Fig. 3, one can clearly observe the increase in lithium content for electrodes with a higher silicon content, with pure graphite at 0% DOD containing 0.46 mg of lithium and 20% silicon containing 1.23 mg of lithium. It is noteworthy that having thicker electrode and consequently higher loading per surface can also lead to higher amount of lithium content presented in the sample, even though the sample has lower silicon content. When comparing the average thicknesses, presented in Table I, it can be seen that the SiG with 10 wt% of silicon is thicker than the samples with higher wt% of silicon and the same applies for the comparison between SiG (15:80) and SiG (20:75). This influences the lithium content of SiG with 10 wt% silicon, which is the reason that the single points of this electrode composition are so close to those of the SiG with 15 wt% silicon. This effect can also be a part of the reason having an outliner at 0% DOD for SiG (15:80). It is also worth to mention that each points from Fig. 3 belongs to the different half-cells built with respective electrode composition and brought to a specific DOD, sums up to 24 separately built half-cells. This is in fact another reason that the one and only outliner should have happened due to some errors in the cell production, since the other half-cells with the same electrode composition but different DODs follow the trend lines.

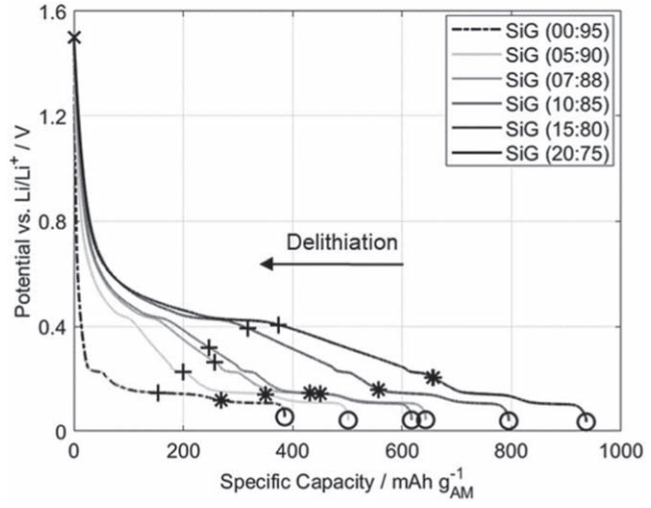

Figure 5. Voltage vs specific capacity for the 1st delithiation of electrodes together with depictions of DODs, at which the electrodes were extracted for NDP measurements.

In Fig. 4 the increase of irreversible capacity in form of inactive lithium situated in the electrode due to SEI formation is shown exemplarily for three different electrode compositions. For higher silicon contents, an increased irreversible capacity is observed. This might originate due to a greater change in volume of the electrodes with high silicon content, where more surface area becomes available for SEI layer growth.

In order to obtain the increase of irreversible capacity from Fig. 4, the SEI formation needs to be investigated. The beginning of the SEI formation was set to meet the reduction potential of the used carbonates and FEC components in the electrolyte. According to Wang et al., FEC already starts reducing when the potential drops under 0.8 V vs Li/Li^+. In this work, we considered the SEI formation from this starting point until the end of the lithiation process.[31] The capacity, which is lost due to trapped lithium in the SEI, is determined in the following steps: by taking the difference of the total lithiation capacity and the capacity at 0.80 V: $Q_1 = Q_{lithi.} - Q_{0.80V}$, to obtain the capacity where SEI growth takes place. In addition, the difference of the obtained capacity Q_l to the capacity at 100% DOD: $\Delta Q = Q1 - Q_{100\%DOD}$, to deduce the reversible quantity of lithium, and hence the capacity lost due to SEI growth. We observe a dependence on the silicon ratio of the active material composition.

(II) NDP analysis.—For the NDP measurements, all electrode samples were fully lithiated from a pristine state before being delithiated to specific DODs. Figure 5 illustrates the DOD points, to which the half cells were first discharged and later measured ex situ using NDP.

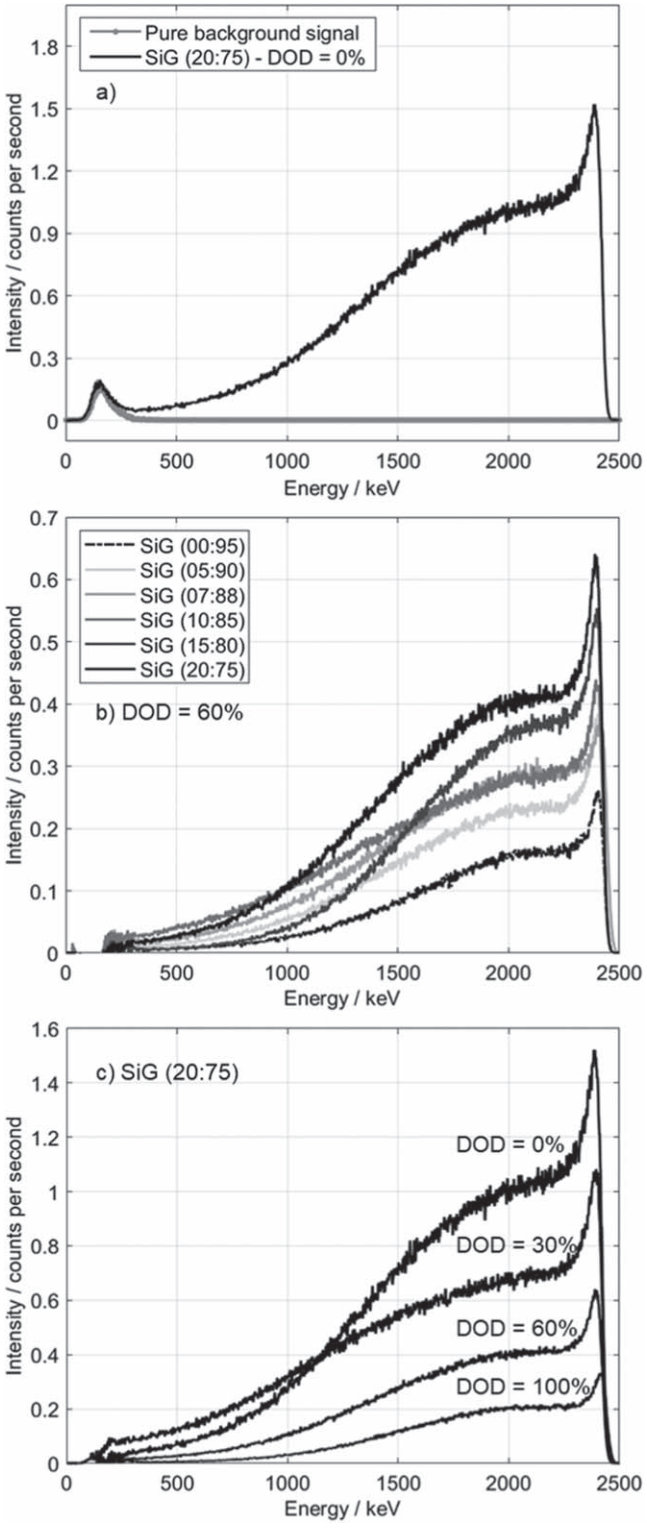

Figure 6. Intensity spectrums: (a) from the SiG (20:75) sample at DOD = 0% together with pure background signal, (b) after background subtraction for different electrode compositions, distinguished using color intensity variation at DOD = 60% and (c) after background subtraction for SiG (20:75) at different DODs.

As an example, NDP data of the 20 wt% silicon SiG electrode taken at 0% DOD is shown in Fig. 6a. As described in the experimental section, the spectrum beginning at ≈ 2.4 MeV shows the energy spectrum of the ^{3}H particles emanating from the electrode after passing through the Kapton® foil. At low energies (below ≈ 500 keV), the

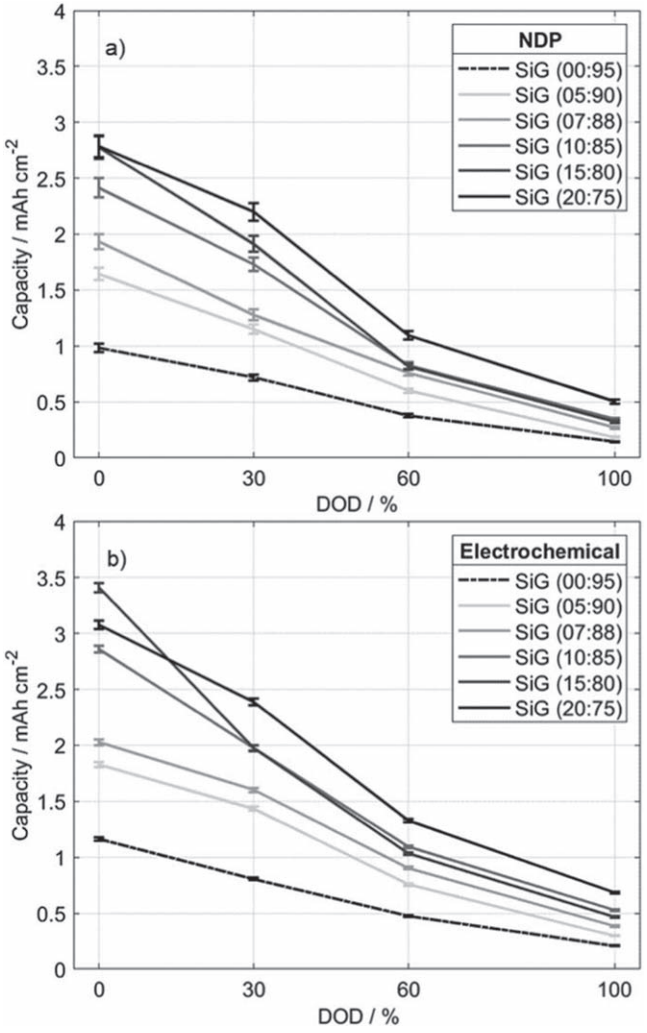

Figure 7. Comparison between capacities derived from (a) NDP data where error bars include statistical uncertainty as well as systematic uncertainty of the reference of ±3.5%[23] and (b) electrochemical data for different SiG electrode compositions at different DODs with a ±1.2% uncertainty.

spectrum is dominated by background originating from β- and γ-radiation from the experimental setup.[25] Also shown is the NDP data obtained from an identical sample without lithium, which serves as reference spectrum for background subtraction for all samples. As an example of the measurement results, in Figs. 6b and 6c, NDP spectra with the background subtracted are shown for different electrode compositions at 60% DOD and SiG (20:75) at different DODs, respectively.

Integration of the NDP spectra gives the total amount of lithium in the electrode, which represents the areal capacity present in the electrodes. In Fig. 7a the areal capacity in form of lithium situated in the electrodes obtained from NDP is shown, whereas the areal capacity derived from the electrochemical analyses is shown in Fig. 7b. A similar plot to Fig. 7b is shown in Fig. 3, where instead of the areal capacity, the inactive lithium amount in mg is shown against the DOD. Areal capacities obtained by NDP and electrochemical analysis (cf. Figs. 7a, 7b) show the same trend and 80 ± 3% of the electrochemically measured capacity is found by NDP as lithium situated in the electrodes. This difference might originate from a possible loss of lithium during electrode extraction, removal of electrolyte residues by electrode washing and sample holder placement prior to the ex situ NDP measurement. In general, an overall higher lithium incorporation with increasing silicon content can be seen with both methods. Furthermore, a lithium depletion

with increased DOD state is observed, as expected. At fully discharged states (100% DOD) the measurements indicate an increasing irreversible capacity with higher silicon content, which originates from irreversible side reactions occurring in silicon-based electrodes. At fully charged state (0% DOD), an areal capacity increase by a factor of ≈ 3 is observed for the 20 wt% compared to that of 0 wt% with both methods. This is in good agreement with the ratio of ≈ 3, when comparing the theoretical capacity of the 20 wt% electrode, i.e. $(0.8 \times 372 + 0.2 \times 3590)$ mAh $g^{-1} = 1016$ mAh g^{-1}, to that of pure graphite as active material, i.e. 372 mAh g^{-1}.

In order to obtain the lithium concentration across the electrode, the energy spectra (Figs. 6b and 6c) are converted to lithium concentration profiles taking into account the energy loss of the ^{3}H particles, as discussed in the experimental section. In Fig. 8a, the resulting lithium concentration profiles for different SiG electrode compositions at different DODs are shown. Furthermore, Figs. 8b and 8c allow a closer look at selected lithium concentration profiles for different SiG electrode compositions at a fixed 100% DOD and a fixed composition of SiG (20:75) at different DODs, respectively. The concentration profiles could be distinguished in three separate parts: (I) The starting point at 0 mg cm^{-2} represents the surface of the harvested electrode, i.e. the interface between the separator and the electrode coating in the coin cell. A lithium peak is observed at the surface, which might originate from the SEI formation around the active material particles. Nevertheless, in NDP it is indistinguishable from a true lithium enrichment.[14] In the latter case, a higher active surface could be available to receive the lithium particles flowing towards the electrode upon lithiation than in the deeper layers of the electrode coating. Another cause of this phenomenon could lie with the lithiation process of the electrodes in the preparation phase, before the NDP measurements. During the preparation phase, the electrodes were brought to different DODs, as discussed in the experimental section. The quantity of lithium that is used to determine the DOD value includes both the (de-)intercalated lithium from the electrode structure, as well as lithium situated on the surface of the electrode. Von Lüders et al.[32] postulates that although there is nearly no chance of lithium plating at lower C-rates, e.g. C/20 as used in this study, electrochemically mobile lithium could still be present on the electrode surface. The electrodes investigated in this work were not calendared, which results in highly uneven electrode coating surfaces. This, in turn, increases the microscopic area given by the sum of all particle surfaces that have contact with the electrolyte and therefore might increase the chance of having a higher amount of deposited lithium on the electrode surface. In addition, having non-calendared electrodes leads to highly porous electrodes, as it is also listed in the Table I of the manuscript. In this way, one can assure that during NDP measurements the beams reached the interface between the current collector and the electrode particles in depth of the electrode coating.

Moreover, greater mass loadings in the concentration profiles indicate the electrode depth going towards the current collector. Part (II) indicates a plateau like profiles, which is homogenous lithium distribution from bulk of the electrodes. This middle region between 0.5 mg cm^{-2} and 3 mg cm^{-2} shows a homogenous lithium distribution for all samples. The lithium concentration profiles are compared at different DODs, in which the 0% DOD represents the fully lithiated state of the electrode (highest lithium concentration) and the 100% DOD represents the fully delithiated state of the electrode compositions (lowest lithium concentration). For the 100% DOD, as one can observe on Fig. 8b), there is an increased SEI formation for higher silicon contents. Since it shows a plateau like profile, the SEI layer is assumed to be formed homogenously. In addition, this concentration plateau in the bulk region indicates a complete and even usage of the bulk of electrode material. Independent on the silicon content, no ionic or electronic transport limitations are found, which would induce an inhomogeneous usage of the electrode. (III) At a mass loading between 4 to 5.5 mg cm^{-2}, a gradual decrease from the surface into the material of the lithium concentration for all measurements is observed. The signal broadening originates from

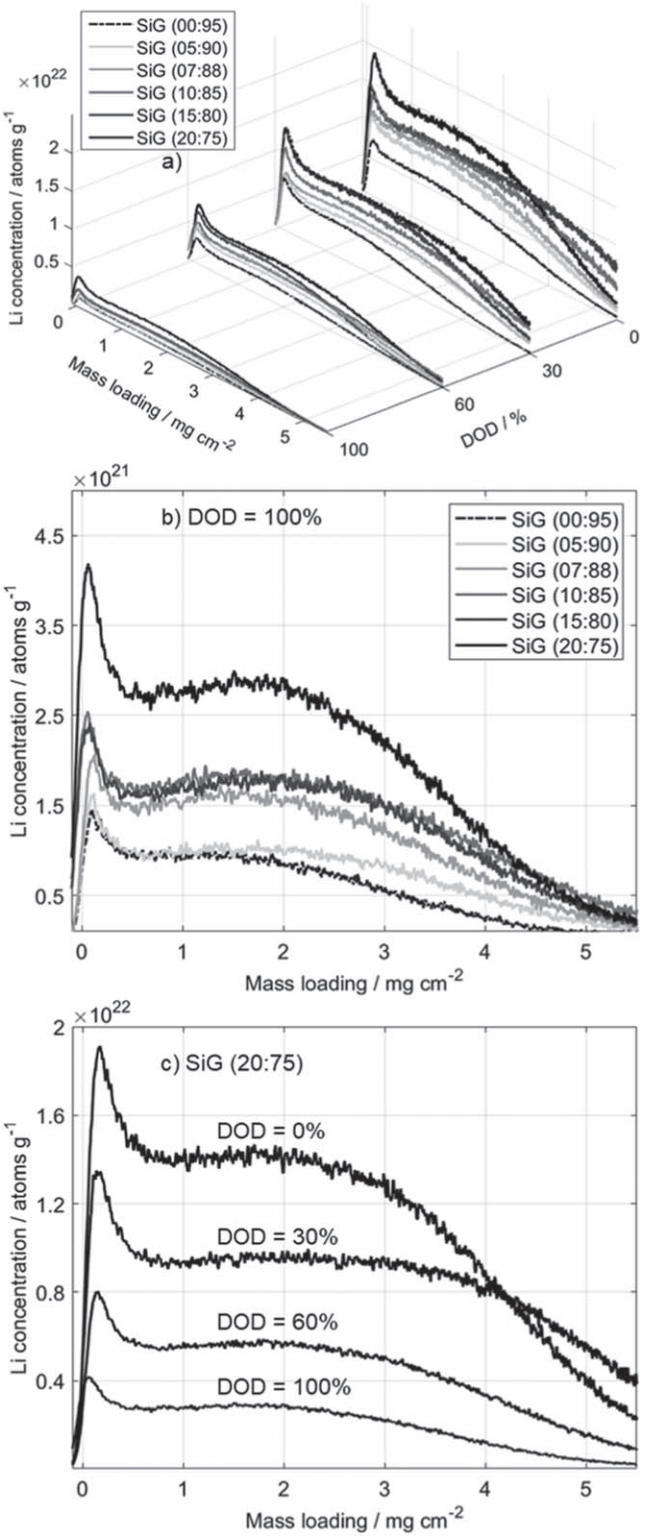

Figure 8. Lithium concentration profiles for: (a) different SiG electrode compositions, distinguished using color intensity variation and at different DODs, (b) different SiG electrode compositions at DOD = 100% and (c) SiG (20:75) at different DODs.

the porous electrode structure and the inflection point represents the interface between electrode coating and current collector (copper foil).[14] The inflection point changes for the different electrodes, since the thicknesses of their coatings vary depending on where the electrodes were punched out from the electrode sheet. Here,

electrodes with coating thicknesses exceeding 40 μm could be measured using NDP compared to previous studies on thin film SiG electrodes.[15]

Considering any single DOD, it can be understood from the profiles, that increasing the silicon content leads to higher concentrations of lithium. In this study, increasing the silicon content in the active material composition from 0 wt% to 20 wt% resulted in an increase of up to 3-times in the content of lithium in the fully lithiated electrode (DOD = 0%). This agrees well with the theoretical capacities and the previous findings from the total areal capacity of the electrodes (Fig. 7). These results corroborate well with previous trends found by Wetjen et al. on a similar system but with a different binder, different silicon contents and a different active to non-active material ratio.[15] We extend the understanding obtained from previous work for a broad range of silicon content and smaller binder compositions. In addition, the results show a stronger but evenly distributed SEI formation on the surface of the electrodes independent of the silicon ratio.

Conclusions

Lithium concentration profiles within SiG composite electrodes containing between 0 wt% and 20 wt% silicon with a beneficial active to non-active material ratio were measured at different DODs using NDP during the first delithiation cycle. A low binder content provides a high specific capacity of the investigated electrodes. Moreover, identical electrode compositions were also investigated after the first full cycle using electrochemical analysis. All NDP findings are in good agreement with the electrochemical results and the whole thicknesses of the electrodes could be investigated using NDP. Areal capacities obtained by NDP and electrochemical analysis show the same trend and NDP shows 80 ± 3% of the electrochemically measured capacity. For both methods, cells were cycled at a low C-rate of C/20 allowing the influence of possible high-C-rate-dependent side reactions to be neglected. Increasing the wt% of silicon in the electrode active material composition leads to higher lithium concentrations and thus higher specific capacities, as expected. Our measurements revealed an increased and homogeneous SEI formation for higher silicon contents for the fully discharged electrodes. For all SiG composite electrodes a homogeneous lithium concentration across the bulk of the electrode is found, indicating a uniform and complete electrode bulk utilization. Even with increasing silicon content, no limiting transport phenomena were found. This work paves the way for further systematic experiments on the impact of silicon content on electrode utilization after extended cycling.

Acknowledgments

The work presented here has received funding from the German Federal Ministry of Education and Research (BMBF) under the grant numbers: 03XP0138B, 03XP0255, 05K19WO8, 05K16WO1 and 03XP0224C. The authors thank the Heinz Maier-Leibnitz Zentrum (MLZ) for providing beam time at FRM II at the PGAA instrument.

Appendix

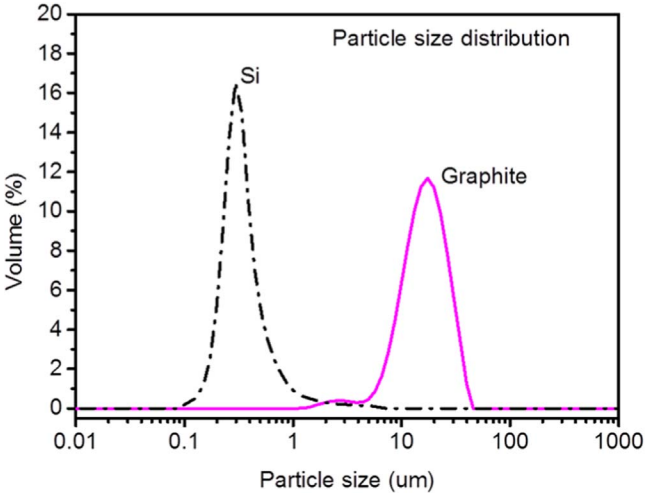

Figure A·1. Particle size distribution of silicon and graphite. The measurement is done using Mastersizer 2000 (Malvern Instruments Ltd., UK).

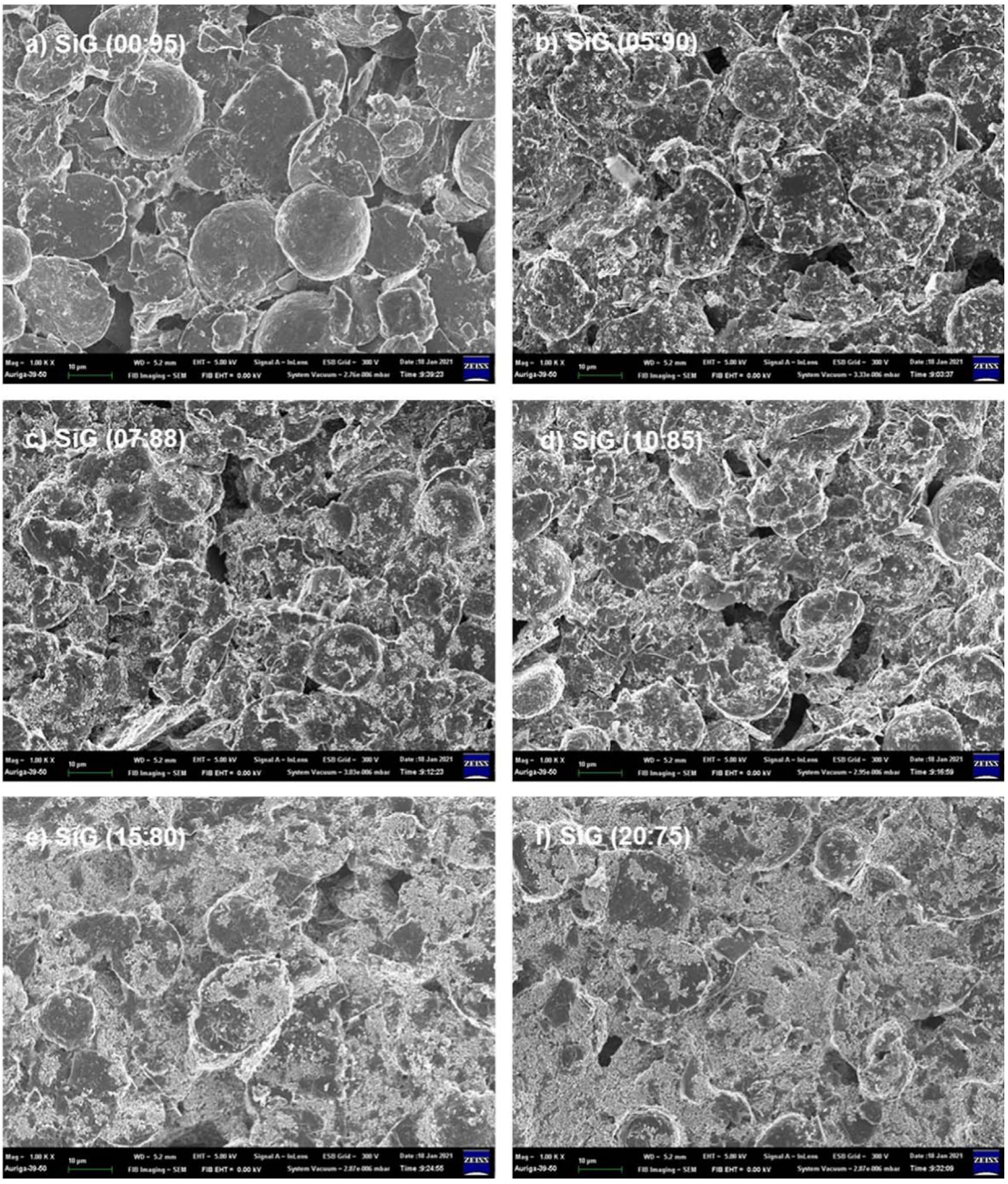

Figure A·2. SEM images of (a) SiG (00:95), (b) SiG (05:90), (c) SiG (07:88), (d) SiG (10:85), (e) SiG (15:80) and (f) SiG (20:75). These analyses are done using ZEISS under $2.76e^{-6}$ mbar, ESB Grid = 300 V, EHT = 5.00 kV and Mag = 1.00 K X. The unit size shown under all single images is 10 μm.

ORCID

Erfan Moyassari https://orcid.org/0000-0002-3037-202X
Andreas Jossen https://orcid.org/0000-0003-0964-1405

References

1. M. Ashuri, Q. He, and L. L. Shaw, "Silicon as a potential anode material for Li-ion batteries: where size, geometry and structure matter." *Nanoscale*, **8**, 74 (2016).
2. J. R. Szczech and S. Jin, "Nanostructured silicon for high capacity lithium battery anodes." *Energy Environ. Sci.*, **4**, 56 (2011).
3. H. Jung, M. Park, Y. G. Yoon, G. B. Kim, and S. K. Joo, "Amorphous silicon anode for lithium-ion rechargeable batteries." *J. Power Sources*, **115**, 346 (2003).
4. M. Winter, J. O. Besenhard, M. E. Spahr, and P. Novak, "Insertion electrode materials for rechargeable lithium batteries." *J. Adv. Mater.*, **10**, 10 (1998).
5. M. N. Obrovac and V. L. Chevrier, "Alloy negative electrodes for li-ion batteries." *Journal of Chemical Reviews*, **114**, 11444 (2014).
6. S. Goriparti, E. Miele, F. De Angelis, E. Di Fabrizio, R. P. Zaccaria, and C. Capiglia, "Review on recent progress of nanostructured anode materials for Li-ion batteries." *J. Power Sources*, **257**, 421 (2014).
7. R. Kumar, A. Tokranov, B. W. Sheldon, X. Xiao, Z. Huang, C. Li, and T. Mueller, "In situ and operando investigations of failure mechanisms of the solid electrolyte interphase on silicon electrodes." *Energy Letters*, **1**, 689 (2016).
8. S. Chae, M. Ko, K. Kim, K. Ahn, and J. Cho, "Confronting issues of the practical implementation of si anode in high-energy lithium-ion batteries." *Joule*, **1**, 47 (2017).
9. H. Wu and Y. Cui, "Designing nanostructured Si anodes for high energy lithium ion batteries." *Nano Today*, **7**, 414 (2012).
10. N. Paul, M. Wetjen, S. Busch, H. Gasteiger, and R. Gilles, *J. Electrochem. Soc.*, **166**, A1051 (2019).
11. N. Paul, H. Frielinghaus, S. Busch, and R. Gilles, "Combining SANS and VSANS to extend Q-range for morphology investigation of silicon-graphite anodes." *Journal Synchrotron Investigation*, **14**, S156 (2020).
12. H. Kim, M. Seo, M. H. Park, and J. Cho, "A critical size of silicon nano-anodes for lithium rechargeable batteries." *Journal of Angewandte Chemie International Edition*, **49**, 2146 (2010).
13. N. Liu, H. Wu, M. T. McDowell, Y. Yao, C. Wang, and Y. Cui, "A yolk-shell design for stabilized and scalable li-ion battery alloy anodes." *Nano Lett.*, **12**, 3315 (2012).

14. M. Trunk, M. Wetjen, L. Werner, R. Gernhäuser, B. Märkisch, Z. Révay, H. A. Gasteiger, and R. Gilles, "Materials science applications of neutron depth profiling at the PGAA facility of heinz maier-leibnitz zentrum." *Journal of Materials Characterization*, **146**, 127 (2018).
15. M. Wetjen, M. Trunk, L. Werner, H. A. Gasteiger, R. Gernhäuser, R. Gilles, B. Märkisch, and Z. Revay, "Monitoring the lithium concentration across the thickness of silicon-graphite electrodes during the first (De-)lithiation." *J. Electrochem. Soc.*, **166**, A1408 (2019).
16. M. Wetjen, D. Pritzl, R. Jung, S. Solchenbach, R. Ghadimi, and H. A. Gasteiger, "Differentiating the degradation phenomena in silicon-graphite electrodes for lithium-ion batteries." *J. Electrochem. Soc.*, **164**, A2840 (2017).
17. D. X. Liu, J. Wang, K. Pan, J. Qiu, M. Canova, L. R. Cao, and A. C. Co, "In situ quantification and visualization of lithium transport with neutrons." *Journal of Angewandte Chemie International Edition*, **53**, 9498 (2014).
18. K. Persson, V. A. Sethuraman, L. J. Hardwick, Y. Hinuma, Y. S. Meng, A. van der Ven, V. Srinivasan, R. Kostecki, and G. Ceder, "Lithium diffusion in graphitic carbon." *J. Phys. Chem. Lett.*, **1**, 1176 (2010).
19. S. Whitney, S. R. Biegalski, Y. H. Huang, and J. B. Goodenough, "Neutron depth profiling applications to lithium-ion cell research." *J. Electrochem. Soc.*, **156**, A886 (2009).
20. J. P. Biersack, D. Fink, R. Henkelmann, and K. Mueller, "The use of neutron induced reactions for light element profiling and lattice localization." *Journal of Nuclear Instruments and Methods*, **149**, 93 (1978).
21. M. Frankenberger et al., "SEI growth impacts of lamination, formation and cycling in lithium ion batteries." *Batteries*, **6**, 21 (2020).
22. S. Lv, T. Verhallen, A. Vasileiadis, F. Ooms, Y. Xu, Z. Li, Z. Li, and M. Wagemaker, "Operando monitoring the lithium spatial distribution of lithium metal anodes." *Nat. Commun.*, **9**, 2152 (2018).
23. D. X. Liu and A. C. Co, "Revealing chemical processes involved in electrochemical (De)lithiation of Al with in situ neutron depth profiling and X-ray diffraction." *Journal of American Chemical Society*, **138**, 231 (2016).
24. Basytec GmbH, *CTS Cell Test System—Technical Specification* (2020), https://basytec.de/prospekte/CTS%202020_04.pdf.
25. L. Werner, M. Trunk, R. Gernhäuser, R. Gilles, B. Märkisch, and Z. Révay, "The new neutron depth profiling instrument N4DP at the Heinz Maier-Leibnitz Zentrum." *Nuclear Instruments and Methods in Physics Research, A*, **911**, 30 (2018).
26. Z. Révay, P. Kudějová, K. Kleszcz, S. Söllradl, and C. Genreith, "In-beam activation analysis facility at MLZ, Garching." *Nuclear Instruments and Methods in Physics Research, A*, **799**, 114 (2015).
27. H. Yuping, R. G. Downing, and H. Wang, "3D mapping of lithium in battery electrodes using neutron activation." *J. Power Sources*, **287**, 226 (2015).
28. NIST, *Certificate of Analysis Standard Reference Material*, **2137** (2010), https://www-s.nist.gov/srmors/certificates/2137.pdf.
29. J. F. Ziegler, M. D. Ziegler, and J. P. Biersack, "SRIM–the stopping and range of ions in matter." *Nuclear Instruments and Methods in Physics Research, B*, **268**, 1818 (2010).
30. B. Key, M. Morcrette, J. M. Tarascon, and C. P. Grey, "Pair distribution function analysis and solid state NMR studies of silicon electrodes for lithium ion batteries: understanding the (de)lithiation mechanisms." *Journal of American Chemical Society*, **133**, 503 (2011).
31. A. Wang, S. Kadam, H. Li, S. Shi, and Y. Qi, "Review on modeling of the anode solid electrolyte interphase (SEI) for lithium-ion batteries." *npj Computational Materials*, **4**, 15 (2018).
32. C. von Lueders, V. Zinth, S. V. Erhard, P. J. Osswald, M. Hofmann, R. Gilles, and A. Jossen, "Lithium plating in lithium-ion batteries investigated by voltage relaxation and in situ neutron diffraction." *J. Power Sources*, **342**, 17 (2017).